

Effect of Process Parameters on the Crack Formation in Laser Metal Powder Deposition of Alloy 718



ANDREAS SEGERSTARK, JOEL ANDERSSON, LARS-ERIK SVENSSON,
and OLANREWAJU OJO

Cracking in Alloy 718 using laser metal powder deposition has been evaluated in this study. It is found that the material is susceptible to cracking when the laser power is high, the scanning speed is high, and the powder-feeding rate is low. Almost all the cracks are located close to the center of the deposited wall and propagate in the normal direction to the substrate. Evidence of liquation are found at the cracked surfaces, and since all cracks reside in regions which are reheated several times, the cracks are determined to most likely be heat-affected zone liquation cracks. The influence of respective process parameter was evaluated using a design of experiment approach. It is shown that, when the powder-feeding rate is incorporated as a variable, the heat input is not a suitable indicator for the hot cracking susceptibility in laser metal powder deposition of Alloy 718. A combinatory model using the power density together with the heat input is therefore proposed.

<https://doi.org/10.1007/s11661-018-4767-0>
© The Author(s) 2018

I. INTRODUCTION

NICKEL (Ni)- and Nickel-iron (Ni-Fe)-based superalloys are widely used in the aero, nuclear, and petrochemical industries due to their capabilities to retain their mechanical properties when used in elevated temperature applications. However, due to the complex chemical composition in these alloys, several secondary phases form in the austenitic γ matrix, which have proven to increase the hot cracking susceptibility of the material.^[1] Due to the rapid precipitation of the strengthening phase γ' in Ni- and Ni-Fe-based superalloys, leading to strain age cracking, many Ni-based superalloys are considered to have low weldability.

The Ni-Fe-based superalloy Alloy 718, on the other hand, is mainly strengthened by the γ'' phase, which has a slower precipitation kinetics compared with the γ' phase. Alloy 718 is therefore considered to have better weldability compared with most of the other Ni-based superalloys. However, in Alloy 718, Laves phase forms through the eutectic reaction $L \rightarrow \gamma + \text{Laves}$ at

approximately 1170 °C, which aids hot cracking susceptibility.^[2] During the deposition of successive layers in laser metal powder deposition (LMPD), the deposited material is reheated multiple times, and much of the deposited material beneath the last layer of deposit constitutes the heat-affected-zone (HAZ) several times, although at different peak temperatures. In the mushy zone of the HAZ, low melting point constituents, such as the Laves phase and MC-carbides are locally melted through eutectic and constitutional liquation reactions, respectively. If the strain, at this point, exceeds a critical value, the liquid separates, and a crack will initiate.^[3]

HAZ liquation cracks have previously been reported in LMPD of Alloy 718 by Chen *et al.*^[4] where they found that a high scanning speed and a high heat input (HI) resulted in a longer total crack length (TCL). In addition, they found that most of the cracks resided at high-angle grain boundaries. Their experiment was conducted with a HI in the range of 300 to 600 J/mm, while the line mass was kept constant throughout the experiment.

Understanding the cracking mechanisms and how to avoid cracking are essential when the size and complexity of the builds increases, as this will lead to an increased complexity of the thermal history which in turn will yield larger thermal stresses acting on the build. In this paper, cracked Alloy 718 samples, produced using a HI of 30 to 50 J/mm, have been microstructurally characterized using optical and electron microscopy. Total crack length (TCL) has been measured

ANDREAS SEGERSTARK, JOEL ANDERSSON and LARS-ERIK SVENSSON are with the Department of Engineering Science, University West, Trollhättan, 461 86, Sweden. Contact e-mail: andreas.segerstark@hv.se OLANREWAJU OJO is with the Department of Mechanical Engineering, University of Manitoba, Winnipeg, R3T 5V6, Canada.

Manuscript submitted December 12, 2017.

Article published online June 28, 2018

from OM images and correlated to processing parameters. , the influences of the powder-feeding rate and the powder focus distance have been considered in order to expand the parameter window for predicting cracking in LMPD of Alloy 718.

II. METHOD AND EXPERIMENT

Thin-walled samples were deposited onto an as-cast Alloy 718 substrate with a thickness of ~ 3 mm. The samples were built using a coaxial nozzle with an annular outlet using a gas-atomized (GA) powder with a size distribution of 20 to 75 μm , low internal porosity, a spherical morphology, and low content of agglomerated satellites. Micrographs of the morphology and cross sections of the powder have previously been reported.^[5] The chemical composition of the powder and substrate are shown in Table I. A 6-kW ytterbium fiber laser that produced an \O 1.6 mm laser spot on the deposition surface was used as energy source. An ABB IRB-4400 robot was used as manipulator for guiding the equipment during deposition. The height of each deposit layer was measured using an optoNCDT1302-20 optical displacement sensor and used as input for the height increment for the successive deposit layer.

A full factorial two-level design of experiment (DoE), here denoted as DoE-A, was used as a screening matrix where laser power, scanning speed, powder-feeding rate, and powder focus (P_{foc}) (a negative value indicates that

the powder spot is focused below the deposition surface and vice versa) are the variable parameters. Each parameter set was repeated three times, resulting in 57 sample runs. The runs were randomly distributed in the design matrix. The parameter sets and the run numbers for the individual sample runs are shown in Table II.

The laser power varied between 400 and 1000 W and the scanning speed varied between 10 and 25 mm/s. This resulted in a range for the HI between 16 and 100 J/mm as calculated using Eq. [1]. The powder-feeding rate varied between 2 and 10 g/min, which resulted in a line mass range of 1.3 to 16.6 mg/mm, calculated using Eq. [2]. The shielding gas flow was kept constant at 11.5 L/min and carrier gas flow was kept at 3 L/min. The parameter settings were adapted from previous reported studies^[6-9] and initial experiments.^[5]

$$\text{HI} = \frac{L_p}{V_s} \quad [1]$$

$$\text{Line mass} = \frac{M_p}{60 V_s}, \quad [2]$$

where L_p is the laser power in Watt, V_s is the scanning speed in mm/s, and M_p is the powder-feeding rate in g/min.

Each sample in the DoE-A contained deposits of four different layer heights, adjacent to each other and mounted in Bakelite sample holders (Figure 1). The first, second, and third deposits were 1-, 2-, and 3 layers

Table I. Chemical Composition in Weight Percent of the GA Alloy 718 Powder and the As-Cast Alloy 718 Substrate

Alloy 718	Fe	Ni	Cr	Nb	Mo	Ta	Ti	Mn	C	B
GA Powder	bal.	52.7	17.5	5.0	3.17	0.003	1.07	0.07	0.031	0.003
As-Cast Substrate	bal.	53.4	18.4	5.2	3.02	—	0.92	0.04	0.046	0.003
	Al	Co	Si	Cu	P	S	Se	Pb	Bi	
GA Powder	0.68	0.2	0.09	0.05	0.006	4.5 (ppm)	1.4 (ppm)	0.09 (ppm)	< 0.05 (ppm)	
As-Cast Substrate	0.48	0.1	0.08	0.02	0.009	0.002	—	—	—	

Table II. The Settings for the Full Factorial Two-Level DoE-A Screening

Parameter Set	Run Number	Lp (W)	Vs (mm/s)	Mp (g/min)	Pfoc (mm)	HI (J/mm)	Cracks
1	6,13,52	400	10	2	- 1	40	no
2	3,9,37	400	10	2	1	40	no
3	30,51,55	400	10	10	1	40	no
4	21,26,32	400	25	10	1	16	no
5	25,41,56	1000	25	10	1	40	no
6	23,35,43	1000	10	2	- 1	100	no
7	33,45,49	1000	25	2	- 1	40	yes
8	14,18,28	1000	25	10	- 1	40	no
9	31,48,54	1000	10	2	1	100	no
10	36,38,47	1000	10	10	1	100	no
11	4,12,15	1000	25	2	1	40	yes
12	7,22,40	1000	10	10	- 1	40	no
13	2,17,42	400	25	2	1	16	no
14	29,44,57	400	25	2	- 1	16	no
15	8,19,27	400	10	10	- 1	40	no
16	5,16,50	400	25	10	- 1	16	no

in the height direction, while the fourth deposit was 15 layers in height. All observed cracks in DoE-A were found in the 15-layer deposits in parameter sets 7 and 11, while no cracks were found in the 1-, 2-, or 3-layer deposits, (Table II).

A new full factorial DoE matrix was designed, concentrating on the parameters that produced the cracked samples in DoE-A. The new matrix is denoted DoE-B. This was done to further evaluate the correlation between process parameters and cracking response. The parameter sets that produced cracks in DoE-A were used as center points in DoE-B (parameter sets 1, 10, and 19) and the parameters were altered ± 10 pct, except for the powder-feeding rate which was altered ± 0.5 g/min (± 25 pct) (Table III). The samples built in DoE-B were of 15 layers in the height direction.

The matrices were designed, and the effects of the process parameters were evaluated using the design of experiment software MODDE®. The values of the

effects of the influential process parameters on TCL were determined and computed as twice the Multiple Linear Regression coefficients.

The cracks were characterized using Olympus BX60M Optical Microscope (OM), FEI Nova Nano-Scanning Electron Microscope (SEM) 450, and a Hitachi TM3000 SEM with a Back Scatter Electron (BSE) detector. Electron Back Scatter Diffraction (EBSD) was performed using a Philips LX30 SEM, coupled with Oxford EBSD detector and analysis system.

The TCL was measured using OM images at 100x magnification. Images were taken from four cross sections for each parameter set.

III. RESULTS

In the screening matrix, cracks were observed in 2 of the 16 parameter sets. The two parameter sets which produced cracks had a high laser power, high scanning speed, but a low powder-feeding rate, and only differed in the powder focus—where one was focused 1 mm above the substrate surface and the other 1 mm below the substrate surface.

A. Crack Characterization DoE-A

Most of the cracks were located close to the center of the deposited walls and propagated in the normal direction to the substrates, (Figure 2(a)). No cracks were found above the uppermost fusion line in the samples, and it can be seen in Figure 2(b) that the cracks stop before the last fusion line. It can also be distinguished that some interlinked secondary phases continues to grow all the way to the fusion line, as indicated by the arrows. This indicates that all cracks were within a region of the samples which at some point of the build constituted the HAZ, of one or more deposited layers. In addition, as no cracks were found in the 1-, 2-, and

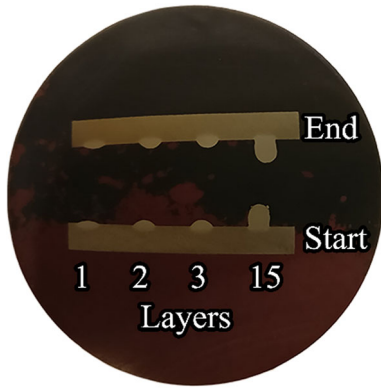


Fig. 1—Example of a deposited sample mounted in Bakelite. Four adjacent thin-walled builds are made for each parameter set that are 1, 2, 3, and 15 layers in height.

Table III. The Parameter Settings for the Full Factorial Two-Level DoE-B Screening

Parameter Set	Lp (W)	Vs (mm/s)	Mp (g/min)	Pfoc (mm)	HI (J/mm)
1	1000	25	2	0	40
2	900	27.5	1.5	-1	33
3	900	27.5	2.5	-1	33
4	900	22.5	1.5	-1	40
5	1100	27.5	2.5	-1	40
6	1100	27.5	1.5	-1	40
7	1100	22.5	1.5	-1	40
8	1100	22.5	2.5	-1	49
9	900	22.5	2.5	-1	49
10	1000	25	2	0	40
11	900	27.5	2.5	1	40
12	900	22.5	2.5	1	33
13	1100	22.5	2.5	1	40
14	900	22.5	1.5	1	49
15	1100	22.5	1.5	1	40
16	1100	27.5	2.5	1	49
17	1100	27.5	1.5	1	40
18	900	27.5	1.5	1	40
19	1000	25	2	0	33

3-layer deposits, it can be concluded that the cracks only first appeared after the deposits were reheated several (at least more than two) times. This also means that no cracks were found where only solidification occurred, without any reheating cycle.

SEM imaging revealed long chains of γ /Laves phase eutectics along the cracked surfaces, (Figure 3). This indicates that the cracks formed at the terminal stage of solidification. Indication of liquation was found using Nano-SEM (Figure 4(a)), where what seems to be re-solidified γ has formed along the cracked grain boundary, similar to what was previously reported by Idowu *et al.*^[10] In addition, what seems to be δ -phase can also be seen at the cracked surface, close to the bottom of the deposit (Figure 4(b)). EBSD revealed that

the cracks were intergranular and resided along high-angle grain boundaries (Figure 5).

B. Effect of Process Parameters on Cracking

From DoE-A, it is seen that a high laser power, high scanning speed, and low powder-feeding rate caused cracking in the 15-layer deposits. However, the parameters that are most influential with respect to cracking length are not well understood from this matrix. A second matrix (DoE-B), closing in on the parameters that caused cracking, was therefore conducted. In this matrix, all parameter sets, except number seven, caused at least some cracking to occur as can be seen in Table IV. The strongest correlation between process

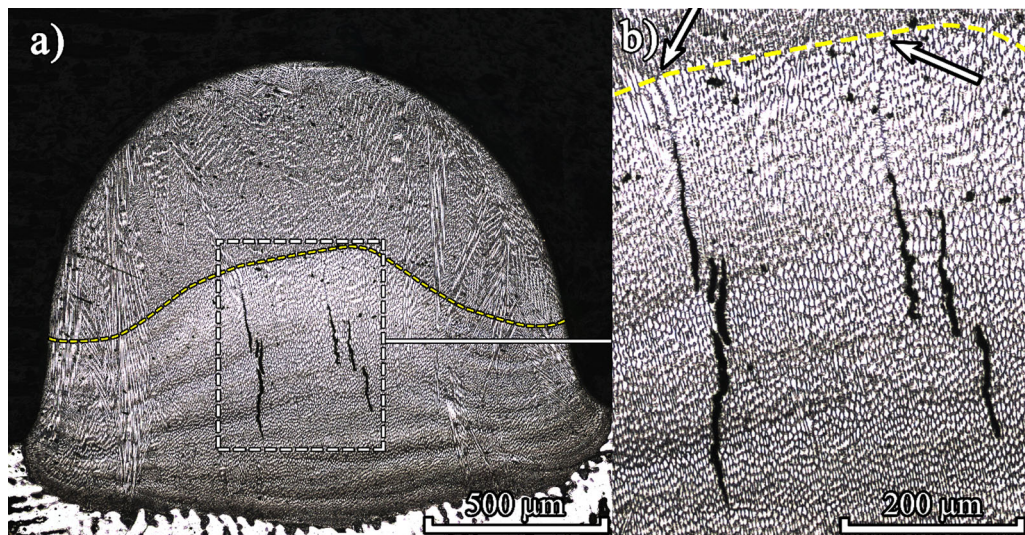


Fig. 2—(a) OM of a cracked cross section. The dashed line indicates the uppermost fusion line. (b) No cracks propagate above the uppermost fusion line. The white arrows indicate where the interlinked secondary phases stop at the last fusion line.

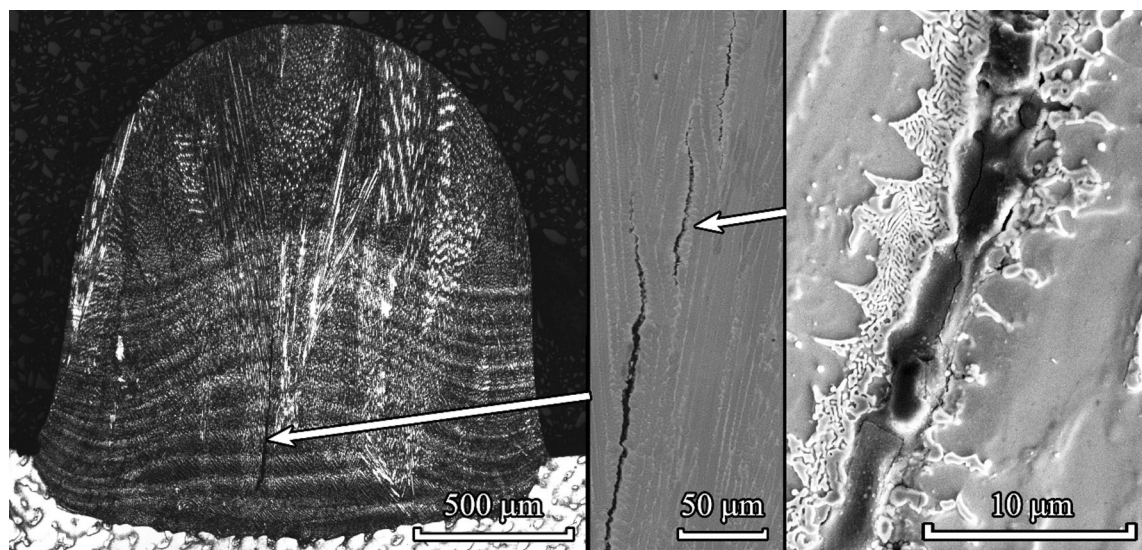


Fig. 3—High-resolution SEM imaging of the cracked area revealing a typical structure of the γ /Laves eutectic adjacent to the crack.

parameters and TCL were found to be powder focus, powder-feeding rate, and laser power as can be seen in Figure 6. This was determined using the statistical toolbox within the design of experiment software MODDE®. Focusing the powder 1 mm above the surface, the increasing powder-feeding rate and the decreasing laser power all contributed to an increased TCL. This is contrary to what was found in DoE-A where the samples with a low powder-feeding rate and high laser power were the samples that exhibited cracking. However, considering the mean values in Figure 7(a), it seems that the TCL increased with the increasing building height. This could indicate that the increased TCL was an effect of longer center-line grain boundaries, within which the cracks could propagate. In

addition, no clear relationship was found between the HI and the TCL, as seen in Figure 7(b).

IV. DISCUSSION

Since no cracks are observed in the 1-, 2-, or 3-layer deposits as well as the absence of cracks in the top of the 15-layer deposit in the initial matrix, no cracks are observed where only solidification occurred without any reheating cycle. It is, therefore, unlikely that solidification cracks are the main cause of the cracks found in the samples. In addition, if any solidification cracking occurred during the build, it would have been re-melted and re-filled when the successive layer was deposited.

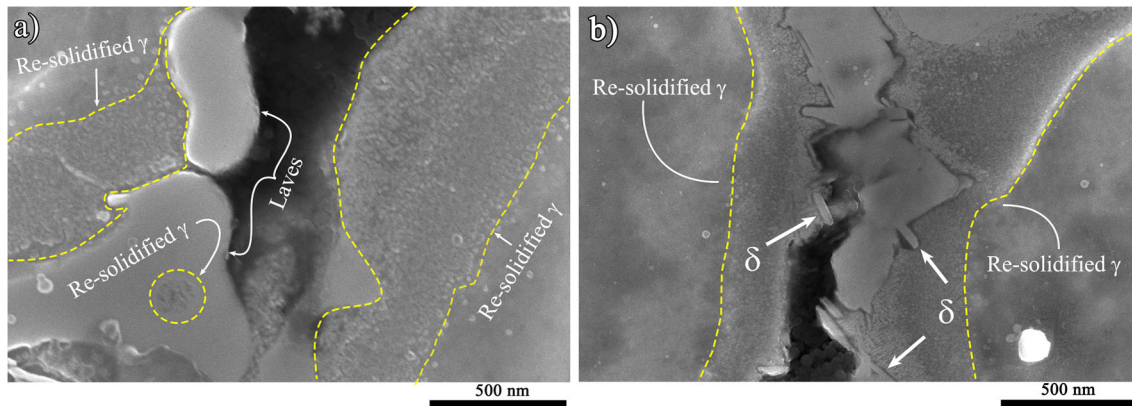


Fig. 4—The seemingly re-solidified γ -phase that can be seen parallel to the crack from the top in (a), to the bottom of the crack, closer to the substrate, in (b). The seemingly δ -phase have also formed in the bottom of the crack as indicated by the white arrows in (b).

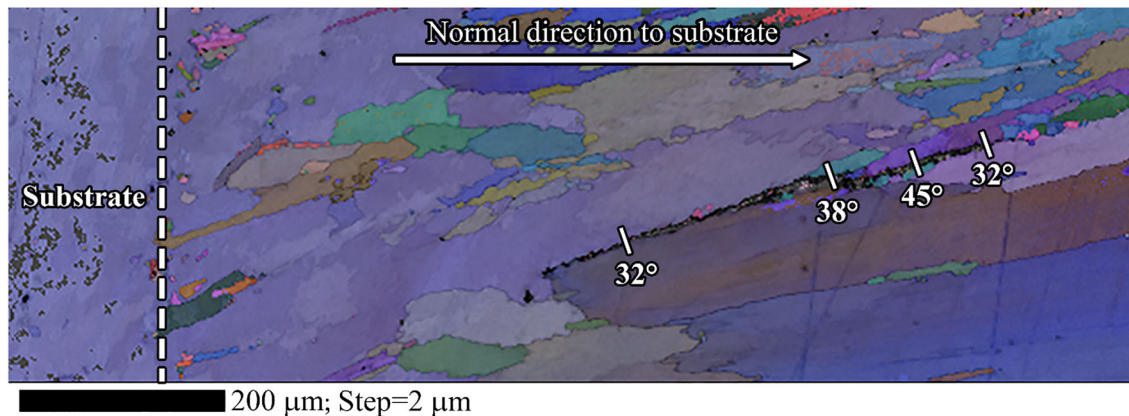


Fig. 5—EBSD of a cracked cross section. Measurements of the boundary angles show that the cracks reside along high-angle grain boundaries.

Table IV. Second DoE Focusing on the Cracking Mechanism Showing Cracking Occurrence in all Samples Except Parameter Set 7

Parameter Set	1	2	3	4	5	6	7	8	9	10
TCL (μm)	1240	560	1440	510	1270	60	0	670	1300	1280
Parameter Set	11	12	13	14	15	16	17	18	19	
TCL (μm)	2070	2230	2010	2030	1520	2350	1050	890	1860	

However, the interlinked γ /Laves phase constituent in the center of the deposit was created during terminal solidification and was a product of segregation in the last remaining liquid. The relatively low melting point of the γ /Laves phase eutectics makes these grain boundaries vulnerable to liquation during successive deposition. It is therefore probable that the cracks were caused by the liquation of these grain boundaries in the HAZ.

In a limited parameter window (DoE-B), it seems that the powder focus and powder-feeding rate are the most influential parameters, most likely due to the higher building rate related to the parameters that generate higher deposits, with longer grain boundaries for the cracks to propagate within. However, this is only the case if the parameters are within a parameter window that generate cracks. All parameter sets, except one, in DoE-B generated cracks, which means that the parameters chosen in the matrix were within a parameter window that promoted cracking. Increasing the laser power within this process window led to a reduced TCL as shown in Figure 6. This means that an increased HI by increasing the laser power does not increase the TCL within this parameter window. In addition, increased HI

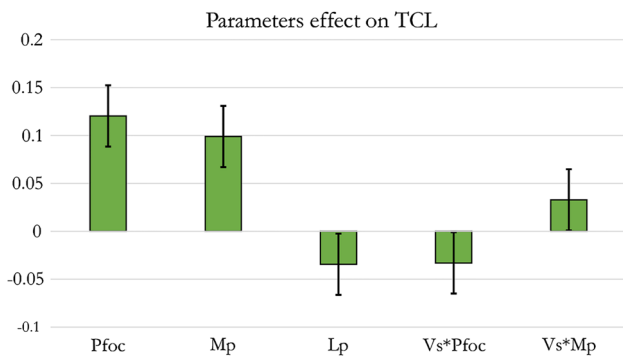
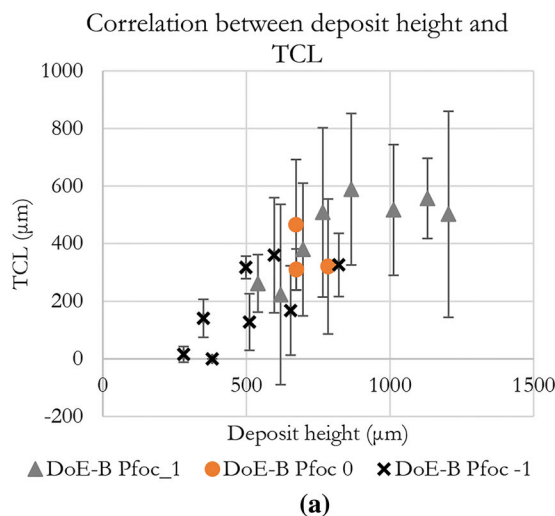


Fig. 6—Diagram showing the process factor's effect of the process parameters in regard to TCL. The effect of the parameters were determined using MODDE®.



by decreasing the scanning speed does not necessarily lead to an increased TCL either. It has been shown that a high scanning speed in welding produces a teardrop shaped weld melt pool that promotes center-line grain boundary segregation, and a high cooling rate which increases the strain in the material. The segregation of alloying elements at the solidification fronts at terminal solidification leads to the formation of γ /Laves eutectic across several layers of deposit. It is probable that the cracks found in the thin substrate samples were located within these types of center-line grain boundaries. In addition, since the line mass were not kept constant in the matrix the decreased scanning speed will increase the line mass which in turn have shown to decrease the melt pool depth and increase the length of the melt pool.^[11] This means that the decrease in weld melt pool length may not be as pronounced when decreasing scanning speed as it would be if the line mass was kept constant.

It is known from DoE-A, that the samples with the highest HI are not necessarily the samples where cracking occur. The cracked cross sections were here

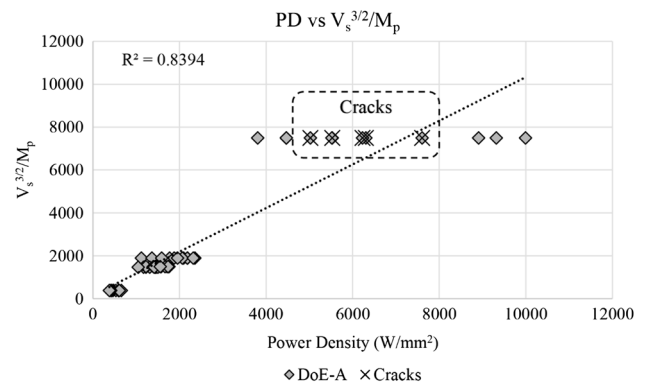


Fig. 8—Observed PD vs predicted PD. The predicted values exhibit a quite good fit with observed PD values at lower values. At higher values (7500W/mm^2), the spread increases significantly. All cracked samples were observed within the samples with the highest PD values.

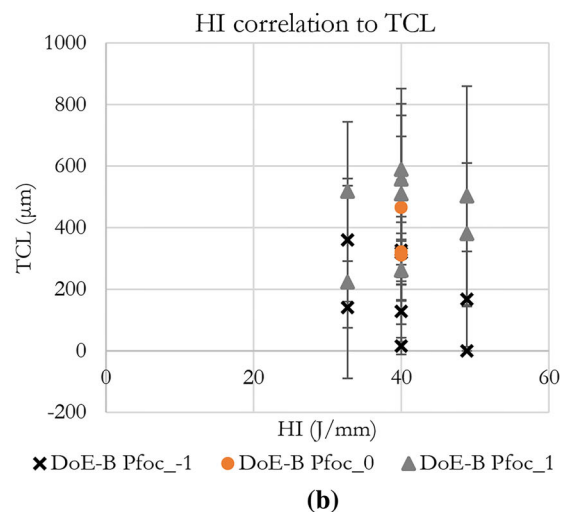


Fig. 7—(a) The building height of the deposit and the correlation to TCL. (b) The influence of HI on TCL.

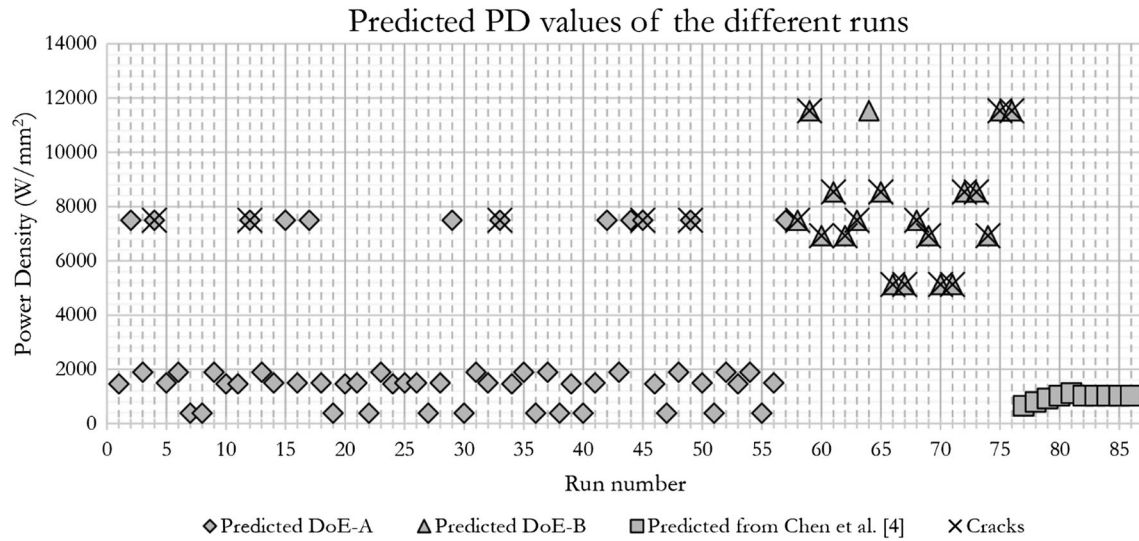


Fig. 9—PD values for different runs. 1 to 57 are the run numbers from DoE-A where the X-markers are the observed cracked samples. 58 to 76 are from DoE-B focusing on the cracked samples, and 77 to 86 are calculated values estimated from Ref. [4].

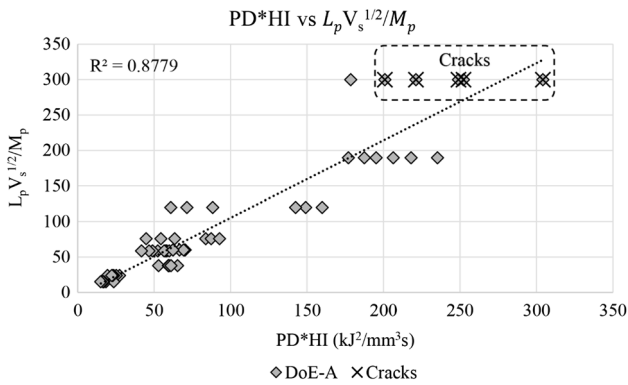


Fig. 10—The correlation between the PD*HI and the TCL. The samples with the highest PD*HI (> 200kJ/mm³s) values seem to be the most prone to crack.

found in the samples with a high laser power, high scanning speed, and low powder-feeding rate, which generate a mid-level HI (40 J/mm) compared with the range of HI in the matrix (16 to 100 J/mm). It is shown in this matrix that through reduced scanning speed, cracks can be avoided while simultaneously increasing the HI. It is further shown that increasing the powder-feeding rate leads to an avoidance of cracking while maintaining the HI at the same level. The HI alone is thus not a suitable indicator of, if the parameters are within a crack susceptible parameter window. In Gas Tungsten Arc welding (GTAW) of austenitic stainless steel a relationship between a Power Density (PD) (Eq. [3]) and cracking was postulated by McCracken and Smith.^[12]

$$PD = \frac{P}{A} \quad [3]$$

where P is the welding power in W and A is the cross section area in mm^2 . This equation is used in GTAW to balance the proportion of weld arc power needed to melt the substrate and the added deposited material in order to control the dilution.^[12] The authors here found that weld cracks were initiated at high PD values. A similar consideration could be suitable in LMPD as both methods use additives to produce the welds, and the materials in both cases have an austenitic matrix with similar cracking mechanisms. The assumption that cracking initiates at a critical PD value was therefore tested using predictive equations. The predicted values were compared to actual values using the measured cross section area from the built samples in DoE-B. The cross-sectional areas of the LMPD deposits were predicted using Eq. [4] which is an empirically constructed equation postulated by El Cheikh *et al.*^[13]

$$A = \alpha \frac{L_p M_p}{60 V_s^{(\frac{3}{2})}} \quad [4]$$

where α is a conversion constant used to fit the model to the experimental data. This conversion constant is needed to correct for variables not accounted for in the equations which could affect the cross-sectional area, such as powder efficiency and laser spot size. In this dataset, α , was set to 0.5 as this provided a good fit with the data. Predicted PD values could then be calculated using Eq. [5].

$$PD = \frac{L_p}{A} = \frac{L_p}{\left(\alpha \frac{L_p M_p}{60 V_s^{(\frac{3}{2})}} \right)} = \frac{60 V_s^{(\frac{3}{2})}}{\alpha M_p} \quad [5]$$

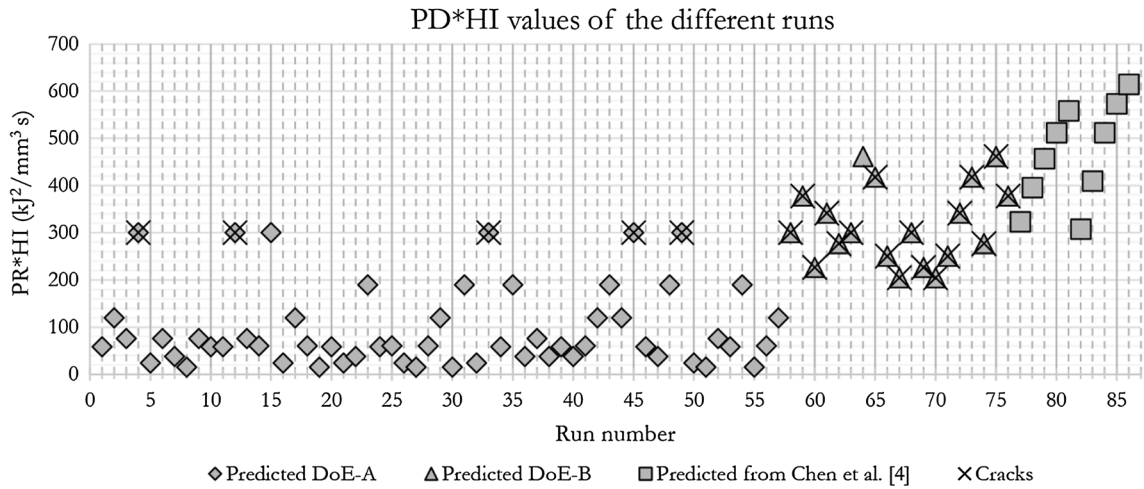


Fig. 11—Predicted PD*HI values for the different runs. 1 to 57 are the run numbers from DoE-A (see Table II) where the X-markers indicate cracked samples. 58 to 76 are from DoE-B (parameter set 1 to 19 in Table III) focusing on the cracked samples, and 77 to 86 are the predicted values estimated from Chen *et al.*^[4] where most of the samples exhibited cracks.

The predicted PD values were compared to the observed PD values for DoE-A, see Figure 8. The observed PD values were calculated using Eq. [3] where the *A* were measured from the cross sections of the samples using OM images. It can be seen here that the predicted PRs correlated quite well with the observed PRs at low values. However, when the PD reached above 3000 W/mm², the fit was quite poor between the observed and the predicted PD values. The cracked runs from DoE-A (see run 4, 12, 33, 45, and 49 in Table II) all exhibited quite high PD values as did the predicted PD from DoE-B (run numbers 58 to 76), see Figure 9. In addition, implementing this equation to the findings of Chen *et al.*^[4] (run numbers 77 to 86) showed that the predicted PD values from their paper were considerably lower than those used in the present study. However, it should be noted that the HIs they used were considerably higher than the HIs used in this study.

It can be seen in Eq. [5] that the decreasing scanning speed and powder-feeding rates could keep the power density at a constant level, while the decreasing scanning speed would increase the HI using Eq. [1]. Therefore, process parameters that produce similar PRs could have vastly different HIs. This suggests a model that includes both the PD and HI when predicting the cracking susceptibility using the process parameters in LMPD. By factoring in the HI, Eq. [6] was attained. As seen in Figure 10, the fit of the parameters that produce the highest PD values were considerably improved. In addition, the cracked samples from Chen *et al.*^[4] are now correlating quite well with the findings in the current study, see Figure 11.

$$PD * HI = \frac{60L_p\sqrt{V_s}}{\alpha M_p} \quad [6]$$

It also seems that PD*HI's correlation to TCL (Figure 12) is stronger than the correlation between HI and TCL (Figure 7(b)). Although the error margin are

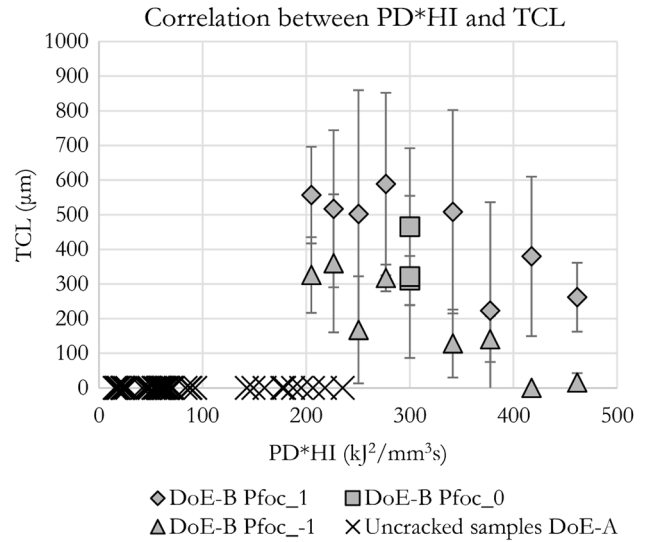


Fig. 12—The correlation between the PD*HI and the TCL.

too wide for any definite conclusions, the mean values indicate that TCL decreases with the increasing PD*HI in this process window (DoE-B). As all cracked samples from DoE-A and DoE-B had high PD*HI values, it is unlikely that the increasing PD*HI generally leads to a reduction in TCL. However, this could be an indication that there is a PD*HI interval where the TCL are the highest and where the increasing PD*HI values beyond a certain peak value leads to a reduction of TCL.

However, it should be noted that the literal factoring of HI may not be the most suitable for predicting cracking susceptibility and should be regarded as a proof of concept. A larger dataset is needed to fully understand how the HI and PD can be combined to formulate a more accurate prediction model. In addition, the deposit shape should be incorporated as it seems that a higher deposit height increases the TCL in the built material.

V. CONCLUSION

The cracking response in LMPD of Alloy 718 has been evaluated and correlated to the process parameters.

- High laser power, high scanning speed, and low powder-feeding rate produced cracks in DoE-A.
- In DoE-B, the longest TCL are observed in the samples with low laser power, low scanning speed, and high powder-feeding rate. Most likely, this was the effect of a higher building rate leading to longer grain boundaries for the cracks to propagate within.
- It is found that the HI is not a suitable parameter to determine the cracking susceptibility when incorporating the powder-feeding rate as a variable.
- The PD is found to predict the cracking response quite well, although it over-estimated the cracking response for parameter sets with a low HI and under-estimated process parameters with a high HI.
- Factoring the HI into the PD increased the fit significantly, which suggests the need of an equation that combines both the PD and HI to predict cracking response in LMPD of Alloy 718. In addition, the building height seems to contribute to the cracking and should therefore be considered in such an attempt.

ACKNOWLEDGMENTS

We thank the Region of Västra Götaland and the Swedish Agency for Economic and Regional Growth for their contribution through funding the project. In addition, we thank GKN Aerospace Sweden AB for their contribution to the project.

OPEN ACCESS

This article is distributed under the terms of the Creative Commons Attribution 4.0 International License (<http://creativecommons.org/licenses/by/4.0/>), which permits unrestricted use, distribution, and reproduction in any medium, provided you give appropriate credit to the original author(s) and the source, provide a link to the Creative Commons license, and indicate if changes were made.

REFERENCES

1. M.J. Donachie and S. Donachie: *Superalloys : A Technical Guide*, 2nd ed., ASM International, Materials Park, 2002.
2. K. Sivaprasad and S. Ganesh Sundara Raman: *Metall. Mater. Trans. A*, 2008, vol. 39A, pp. 2115–27.
3. W. Pellini: *Foundry*, 1952, vol. 80, pp. 125–33.
4. Y. Chen, K. Zhang, J. Huang, S.R.E. Hosseini, and Z. Li: *Mater. Des.*, 2016, vol. 90, pp. 586–94.
5. A. Segerstark, J. Andersson, and L.-E. Svensson: *Opt. Laser Technol.*, 2017, vol. 97, pp. 144–53.
6. G.K.L. Ng, A.E.W. Jarfors, G. Bi, and H.Y. Zheng: *Appl. Phys. A*, 2009, vol. 97, pp. 641–49.
7. Q.-L. Zhang, J.-H. Yao, and J. Mazumder: *J. Iron Steel Res. Int.*, 2011, vol. 18, pp. 73–78.
8. C. Hong, D. Gu, D. Dai, A. Gasser, A. Weisheit, I. Kelbassa, M. Zhong, and R. Poprawe: *Opt. Laser Technol.*, 2013, vol. 54, pp. 98–109.
9. K. Zhang, W. Liu, and X. Shang: *Opt. Laser Technol.*, 2007, vol. 39, pp. 549–57.
10. O.A. Idowu, O.A. Ojo, and M.C. Chaturvedi: *Mater. Sci. Eng. A*, 2007, vols. 454–455, pp. 389–97.
11. K. Shah, A.J. Pinkerton, A. Salman, and L. Li: *Mater. Manuf. Processes*, 2010, vol. 25, pp. 1372–80.
12. S. L. McCracken and R. E. Smith: in *Hot Cracking Phenomena in Welds III: Behavior and Hot Cracking Susceptibility of Filler Metal 52 M (ERNiCrFe-7A) Overlays on Cast Austenitic Stainless Steel Base Materials*, T. Böllinghaus, J. Lippold, and C. E. Cross, eds., Springer, Berlin Heidelberg, 2011, pp. 333–52.
13. H. El Cheikh, B. Courant, S. Branchu, J.-Y. Hascoët, and R. Guillén: *Opt. Lasers Eng.*, 2012, vol. 50, pp. 413–22.